Journal of Medicinal Chemistry

Article

4-(((4-Iodophenyl)methyl)-4H-1,2,4-triazol-4-ylamino)-benzonitrile: A potential imaging agent for aromatase

Jin Song, Zehui Wu, Phumvadee Wangtrakuldee, Seok Rye Choi, Zhihao Zha, Karl Ploessl, Robert H. Mach, and Hank F. Kung

J. Med. Chem., **Just Accepted Manuscript** • DOI: 10.1021/acs.jmedchem.6b00849 • Publication Date (Web): 02 Oct 2016

ACS Publications

Journal of Medicinal Chemistry is published by the American Chemical Society. 1155 Sixteenth Street N.W., Washington, DC 20036

4-(((4-Iodophenyl)methyl)-4H-1,2,4-triazol-4-ylamino)-benzo nitrile: A potential imaging agent for aromatase

Jin Song[1,2], Zehui Wu[2], Beau Wangtrakuldee[3], Seok Rye Choi[2,4], Zhihao Zha[2], Karl Ploessl[2,4], Robert H Mach[2], Hank Kung*[1,2,4]

[1]Beijing Institute for Brain Disorders, Capital Medical University, Beijing, 100069, China

[2]Department of Radiology, University of Pennsylvania, Philadelphia, 3700 Market Street, Suite 305, Pennsylvania 19104

[3]Department of Systems Pharmacology and Translational Therapeutics and the Center for Excellence in Environmental Toxicology, Perelman School of Medicine, University of Pennsylvania, 1315 BRBII/III, 421 Curie Blvd, Philadelphia, PA 19104-6160

[4]Five Eleven Pharma Inc., Philadelphia, PA 19104

Abstract

Aromatase (CYP19) is a rate-limiting enzyme that catalyzes the biosynthesis of estrogens. Imaging agents based on aromatase inhibitors (AIs) has been developed for a PET/SPECT study. A series of compounds was synthesized based on YM511, which has previously been used for breast cancer treatment. Two examples of these derivatives, 4-(((4-iodophenyl)methyl)-4H-1,2,4-triazol-4-yl-amino)-benzonitrile (**5**) and 4-((1H-imidazol-1-yl)(4-iodobenzyl)amino)benzonitrile (**11**), displayed potent binding affinities to human aromatase (IC_{50} = 0.17 and 0.04 nM, respectively). Biodistribution and autoradiographic studies revealed that [^{125}I]**5** and [^{125}I]**11** were highly accumulated in the stomach (16.21 and 10.88% dose/g, respectively) and ovaries (8.56 and 3.32% dose/g, respectively) of female rats. Log P of [^{125}I]**5** was 2.49, meaning good brain penetration. Autoradiograms of brain sections showed a high uptake in the bed nucleus of the stria terminalis and amygdala. These results suggest that [^{125}I]**5** and [^{125}I]**11** are potent probes for aromatase imaging in both the brain and peripheral organs.

Introduction

Aromatase, the product of the CYP19 gene (also known as estrogen synthetase or estrogen synthase), is the obligatory enzyme catalyzing the biosynthesis of estrogens from androgen precursors. It is a cytochrome P450 protein of the 19A family, also known as P450AROM estrogen synthase.[1] Aromatase is widely distributed in peripheral organs such as the ovaries,[2] skin,[3] adipose tissue[4] as well as the brain.[5] Aromatase has been reported overexpressed in women diagnosed with breast cancer,[6] endometriosis,[7] and liver cancer.[8] Brain aromatase is involved in regulating sexual behavior, aggression, cognition, memory, and neuroprotection.[9] It has been reported that the aromatase immunoreactivity changed during the pathophysiology of Alzheimer's disease.[10]

Aromatase inhibitors (AIs) have been increasingly used in the hormonal treatment of breast cancer.[11, 12] The aromatase inhibitors fall into two categories: **A**) steroidal AIs such as formestane and exemestane, which bind irreversibly to the active site in aromatase, and **B**) non-steroidal AIs such as aminoglutethimide, fadrozole, anastrozole, letrozole, and vorozole, whose binding is competitive and reversible to the active site in aromatase.[11] Several AIs, including vorozole, letrozole, and cetrozole have been labeled with ^{11}C.[13-16] [^{11}C]vorozole was the first aromatase radiotracer used in human brain

studies and has been well-studied in rodents, primates, and humans. It accumulated highly in the amygdala and hypothalamic areas of the brain[14, 17, 18] as well as in rat stomach.[15] Because of the absence of regional specificity, [^{11}C]letrozole was deemed unsuitable as a PET radiotracer for brain aromatase.[13] Recently, [^{11}C]cetrozole has been reported to show high specific binding in the amygdala, hypothalamus, and nucleus accumbens of rhesus monkeys with a higher signal-to-noise ratio than [^{11}C]vorozole.[19] However, the existing ^{11}C radiotracers for aromatase imaging showed several disadvantages. It is difficult to synthesize the precursor of [^{11}C]vorozole, and the nonspecific signal in PET imaging is high.[19] Although [^{11}C]cetrozole showed a higher signal to noise ratio, its radiosynthesis is difficult. The PET imaging study of ^{18}F-labeled vorozole, 6-[(S)-(4-chlorophenyl)(1H-1,2,4-triazol-1-yl)methyl]-1-(2-[^{18}F]fluoroethyl)-1H-benzotriazole, in monkey brains also showed high non-specific binding.[20]

YM511, an aminotriazole derivative, and a non-steroidal aromatase inhibitor, has been used for the treatment of breast cancer in postmenopausal women. The early phase II study of YM511 appeared to be effective and safe in postmenopausal patients with breast cancer.[21] However YM511 was abandoned due to competitive market reasons.[22] YM511 has a high binding affinity to human aromatase and a simple structure that is easy to synthesize. It has potential to be a good PET/SPECT imaging agent of aromatase. Moreover, the binding patterns of aromatase tracers in peripheral organs need further study. In order to explore new tracers with potentially better in vivo characteristics for aromatase imaging, we synthesized a series of compounds, radiolabeled them with I-125,

and investigated regional patterns of their specific binding through in vivo and ex vivo experiments.

Results

Chemical synthesis. In order to develop [^{123}I] SPECT imaging agents, **5, 8 and 11** were synthesized according to schemes 1, 2, and 3. Ligands **5, 8, and 11** were derived from YM511 (**1a**),[23] **6a,**[24] and **9**[25] respectively, ligands which have been reported to show high binding affinities to aromatase. The synthesis of **1a-c** was accomplished by the reactions described in Scheme 1. These reactions followed methods reported in the literature. Compound **4** was prepared by reacting **1a** with bis(tributyltin). Ligand **4** was treated with iodine to give **5**. Ligands **6a-b** and **9** were prepared by a method similar to the reported procedure.[25] Ligands **8** and **11** were prepared in similar fashion as ligand **5.** In order to develop [^{18}F]-labeled PET imaging agents, **3a** and **b** were synthesized according to Scheme 1. Ligand **1c** was treated with BBr_3 to give **2.** Ligand **2** was then treated with either 1-bromo-2-fluoro-ethane or 3-fluoropropyl 4-methylbenzenesulfonate to give **3a** or **3b**.

Two high performance liquid chromatography (HPLC) conditions were performed to test the purity of the final compounds, **3a**, **3b**, **5**, **8**, and **11**. An Agilent HPLC 1100 series with **A**) a 5 μm C18 250 mm × 10 mm column, eluted with ACN/10 mM ammonium formate buffer, 6/4, 3 mL/min or **B**) a 5 μm C18 250 mm × 10 mm column, eluted with MeOH/10 mM ammonium formate buffer, 7/3, 3 mL/min. All of the final tested samples showed a purity > 95%. The HPLC profiles are included in the supplementary information.

Scheme 1: Synthesis of (4-benzyl(4*H*-1,2,4-triazol-4-yl)amino)benzonitrile derivatives

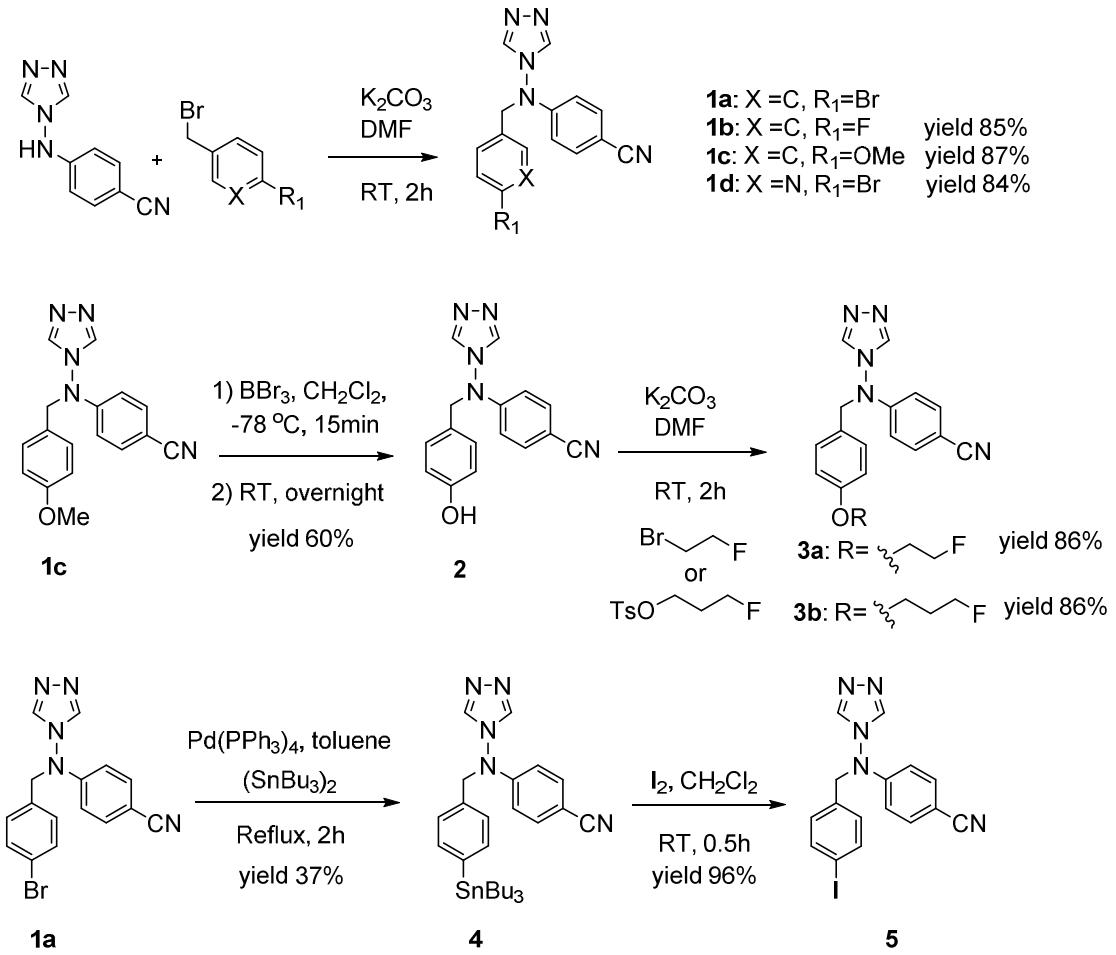

Scheme 2. Synthesis of 4-((4-iodobenzyl)(pyrimidin-5-yl)amino)benzonitrile

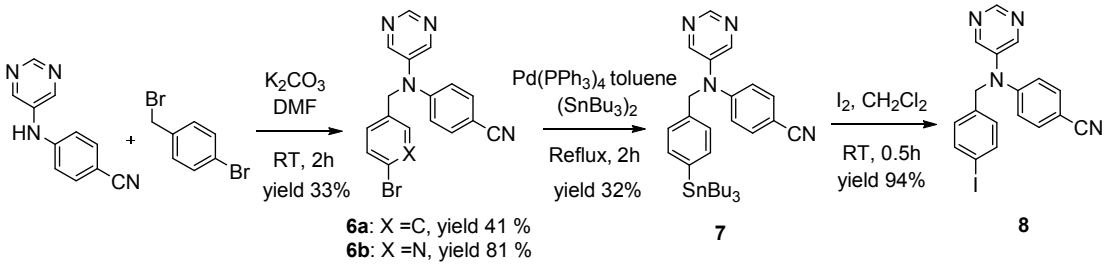

Scheme 3. Synthesis of 4-((1H-imidazol-1-yl)(4-iodobenzyl)amino)benzonitrile

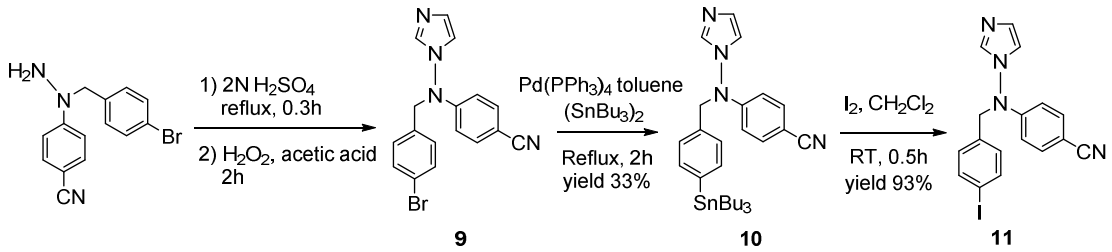

In vitro binding assays to human CYP19 (aromatase). An in vitro binding assay was employed to measure the inhibition of the new compounds to [^{125}I]**5** binding to human CYP19. The half maximal inhibitory concentrations (IC_{50}, nM) of the new compounds against the binding to human CYP19 are shown in **Table 1**. High binding affinities were obtained for several compounds. The ligands 4-((4-iodobenzyl)(4H-1,2,4-triazol-4-yl)amino) benzonitrile (**5**), 4-((4-iodobenzyl)(pyrimidin-5-yl)amino)benzonitrile (**8**) and 4-((1H-imidazol-1-yl)(4-iodobenzyl)amino)benzonitrile (**11**), showed excellent binding affinities (IC_{50} = 0.17, 0.04, and 0.04 nM, respectively), compared to YM511 (IC_{50} = 0.32 nM). However, ligands **3a** and **6b** showed a significantly lower affinity (IC_{50} = 40.2 and 11.6 nM, respectively), and the ligand **3b** also showed dramatically low binding affinity (IC_{50} = 273 nM).

Table 1. Comparison of the half maximal inhibitory concentration (IC_{50}) of the human CYP19 (aromatase) targeting ligands against [^{125}I]5 binding to human CYP19.

compd	IC_{50} (nM)	compd	IC_{50} (nM)	compd	IC_{50} (nM)
YM511	0.32 ± 0.07	**1c**	5.06 ± 0.42	**6a**	0.06 ± 0.02
Letrozole	7.56 ± 1.79	**1d**	2.88 ± 0.27	**6b**	11.6 ± 3.50
Anastrozole	7.98 ± 1.93	**3a**	40.2 ± 12.3	**8**	0.04 ± 0.03
Fadrozole	1.14 ± 0.09	**3b**	273 ± 23	**9**	0.93 ± 0.48

Exemestane	318 ±133	**5**	0.17 ± 0.05	**11**	0.04 ± 0.02

n = 4. Values were obtained from the mean ± SD of four independent experiments, each in duplicates.

Radiolabeling of 4-((4-iodobenzyl)(4H-1,2,4-triazol-4-yl)amino)benzonitrile, 4-((4-iodobenzyl)(pyrimidin-5-yl)amino)benzonitrile, and 4-((1H-imidazol-1-yl)(4-iodobenzyl)amino)benzonitrile. The radioiodinated ligand, [^{125}I]5, was prepared from the corresponding tributyltin precursor, **4**, by an iododestannylation reaction (see Scheme 4). After the reaction was terminated, HPLC purification was performed on a 5 μm C18 250 mm × 4.6 mm column. Radiochemical yield was 57% (decay corrected (dc)) with a radiochemical purity of >99% after HPLC purification. The radiochemical identity of the radioiodinated ligand was verified by a co-injection of the "cold compound", **5** (see Figure 1). The radiolabeling of [^{125}I]**8** (RCY 63% (dc); RCP >99%) and [^{125}I]**11** (RCY 61% (dc); RCP >99%) were successfully performed using the same protocol as [^{125}I]**5**. The same procedure will be suitable for preparation of ^{123}I labeled agents, which are suitable for SPECT imaging.

Scheme 4. Radiosynthesis of [^{125}I]5, [^{125}I]8 and [^{125}I]11

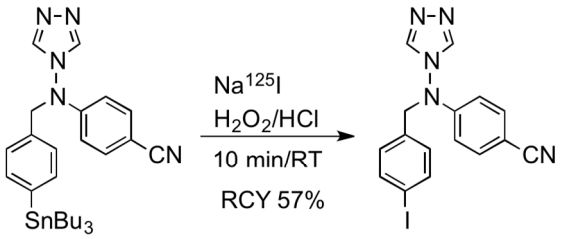

4 **[^{125}I]5**

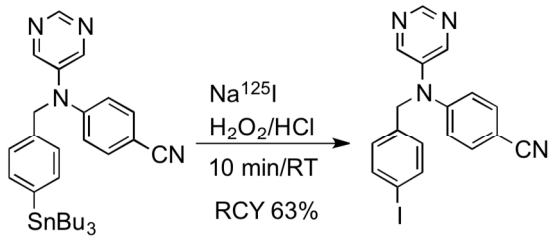

7 **[^{125}I]8**

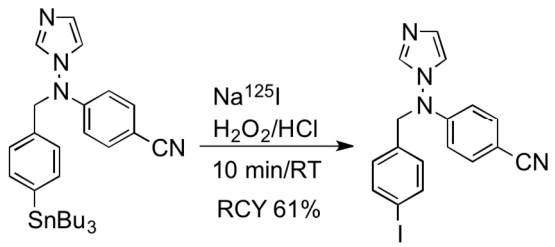

10 **[^{125}I]11**

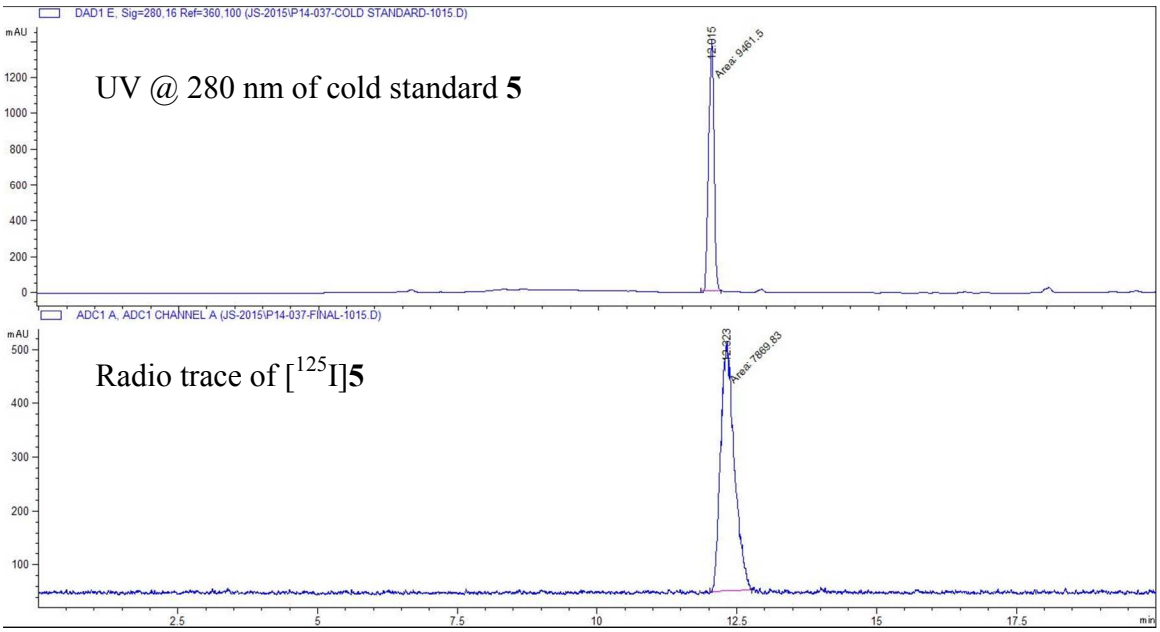

Figure 1. HPLC profiles of cold standard **5** and [^{125}I]**5** on a 5 µm C18 250 mm × 4.6 mm column with the following gradient and a flow rate: 1 mL/min, 0-15 min ammonium formate buffer (10 mM) 90 to 0%, ACN 10-100%; 15-20 min ACN 100%.

Partition coefficient (Log P). Partition coefficients between 1-octanol/buffer of [^{125}I]**5**, [^{125}I]**8,** and [^{125}I]**11** were determined to be 2.49, 2.16, and 1.59, respectively. According to Hansch and co-workers' study[26, 27], optimum CNS penetration approximately Log P = 2 ± 0.7, meaning the lipophilicity of the three compounds is suitable for imaging aromatase activity in the CNS.

In vivo biodistribution. As shown in Table 2, [^{125}I]**5**, [^{125}I]**8,** and [^{125}I]**11** showed high uptakes in the stomach at 60 min post-injection, with [^{125}I]**5** showing the highest uptake among the three ligands (16.21 ± 0.62% dose/g). The female rats displayed significantly higher [^{125}I]**5** uptake in the stomach than male rats **(**16.21 vs. 10.12% dose/g, P = 0.002**)**. [^{125}I]**8** and [^{125}I]**11** also showed higher stomach uptake, 6.29 vs. 4.86% dose/g for [^{125}I]**8** and 10.8 vs. 4.90% dose/g for [^{125}I]**11**, respectively. The uptake

in ovaries at 60 min post-injection was also high, 8.56 ± 3.79% dose/g for [^{125}I]**5**, 2.25 ± 0.49% dose/g for [^{125}I]**8** and 3.32 ± 0.11% dose/g for [^{125}I]**11**, respectively. There was no uptake in the testes for all three ligands. The liver and adrenal glands also showed uptake to varying degrees. However, radioactivity levels in liver and adrenal glands were not changed by pre-treatment of anastrozole (2 mg/kg, iv, data not shown), suggesting that the binding was non-specific.

Table 2.1. Comparison of biodistribution of [^{125}I]5, [^{125}I]8, and [^{125}I]11 in normal rats (% dose/g)

	[^{125}I]**5**		[^{125}I]**8**		[^{125}I]**11**	
Organ	**Female**	**Male**	**Female**	**Male**	**Female**	**Male**
Blood	0.32 ± 0.03	0.43 ± 0.07	0.54 ± 0.10	0.43 ± 0.06	0.21 ± 0.03	0.24 ± 0.03
Heart	0.62 ± 0.01	0.57 ± 0.01	0.28 ± 0.03	0.21 ± 0.01	0.37 ± 0.01	0.23 ± 0.04
Muscle	0.30 ± 0.02	0.29 ± 0.01	0.13 ± 0.02	0.14 ± 0.00	0.17 ± 0.01	0.12 ± 0.01
Lung	0.52 ± 0.02	0.49 ± 0.01	0.34 ± 0.05	0.26 ± 0.02	0.38 ± 0.03	0.28 ± 0.03
Kidneys	0.77 ± 0.02	0.81 ± 0.01	0.75 ± 0.02	0.60 ± 0.03	1.10 ± 0.09	0.59 ± 0.11
Spleen	0.42 ± 0.02	0.38 ± 0.01	0.17 ± 0.02	0.15 ± 0.03	0.32 ± 0.04	0.18 ± 0.03
Pancreas	0.82 ± 0.02	0.67 ± 0.02	0.68 ± 0.04	0.52 ± 0.23	0.81 ± 0.07	0.37 ± 0.04

Liver	3.37 ± 0.15	2.77 ± 0.04	1.32 ± 0.05	0.99 ± 0.09	3.93 ± 0.16	7.47 ± 1.67
Skin	0.21 ± 0.02	0.26 ± 0.18	0.26 ± 0.03	0.31 ± 0.04	0.28 ± 0.05	0.19 ± 0.03
Brain	0.31 ± 0.01	0.26 ± 0.01	0.12 ± 0.01	0.08 ± 0.01	0.27 ± 0.02	0.14 ±0.02
Thyroid	0.51 ± 0.02	0.54 ± 0.01	0.69 ± 0.04	0.48 ± 0.26	0.58 ± 0.06	0.33 ± 0.09
Adrenal glands	1.06 ± 0.09	0.88 ± 0.06	1.83 ± 0.35	1.13 ± 0.15	2.11 ± 0.16	1.20 ± 0.14
Stomach	16.21 ± 0.62	10.12 ± 0.04	6.29 ± 0.59	4.86 ± 0.22	10.88 ± 1.97	4.90 ± 0.91
Intestine	0.65 ± 0.04	0.49 ± 0.46	0.92 ± 0.10	0.86 ± 0.22	0.85 ± 0.07	0.57 ± 0.16
Ovaries/ Testes	8.56 ± 3.79	0.35 ± 0.04	2.25 ± 0.49	0.41 ± 0.08	3.32 ± 0.11	0.34 ± 0.06

Table 2.2. In vivo blocking study (% dose/g)

	[^{125}I]**5**		[^{125}I]**8**		[^{125}I]**11**	
Organ	**Female**	**Male**	**Female**	**Male**	**Female**	**Male**
Blood	0.36 ± 0.01	0.39 ± 0.02	0.54 ± 0.03	0.43 ± 0.06	0.24 ± 0.01	0.26 ± 0.03
Heart	0.81 ± 0.02	0.71 ± 0.03	0.34 ± 0.02	0.26 ± 0.02	0.48 ± 0.04	0.29 ± 0.00
Muscle	0.38 ± 0.01	0.36 ± 0.02	0.16 ± 0.01	0.17 ± 0.01	0.23 ± 0.01	0.14 ± 0.01
Lung	0.64 ± 0.03	0.58 ± 0.02	0.39 ± 0.03	0.28 ± 0.03	0.49 ± 0.04	0.32 ± 0.02
Kidneys	0.95 ± 0.03	1.11 ± 0.14	0.96 ± 0.08	0.94 ± 0.03	1.40 ± 0.17	0.89 ± 0.04
Spleen	0.53 ± 0.03	0.47 ± 0.05	0.27 ± 0.06	0.15 ± 0.01	0.38 ± 0.03	0.23 ± 0.03
Pancreas	0.97 ± 0.06	0.85 ± 0.08	0.95 ± 0.08	0.59 ± 0.14	0.96 ± 0.06	0.55 ± 0.02

Liver	3.66 ± 0.68	3.49 ± 0.58	1.60 ± 0.35	1.18 ± 0.19	4.72 ± 0.69	8.48 ± 1.20
Skin	0.26 ± 0.02	0.30 ± 0.01	0.29 ± 0.03	0.36 ± 0.01	0.27 ± 0.07	0.22 ± 0.02
Brain	0.37 ± 0.01	0.32 ± 0.01	0.16 ± 0.02	0.10 ± 0.01	0.38 ± 0.03	0.18 ±0.02
Thyroid	0.63 ± 0.03	0.66 ± 0.08	0.61 ± 0.08	0.50 ± 0.04	0.58 ± 0.03	0.39 ± 0.05
Adrenal glands	1.23 ± 0.12	1.12 ± 0.09	1.90 ± 0.21	1.60 ± 0.19	2.63 ± 0.17	1.55 ± 0.09
Stomach	0.69 ± 0.03	0.63 ± 0.05	0.45 ± 0.04	0.35 ± 0.01	1.57 ± 0.11	0.67 ± 0.55
Intestine	0.74 ± 0.04	0.63 ± 0.06	1.11 ± 0.27	0.87 ± 0.24	1.15 ± 0.03	0.84 ± 0.03
Ovaries/ Testes	0.70 ± 0.03	0.37 ± 0.04	0.97 ± 0.14	0.40 ± 0.10	1.20 ± 0.21	0.41 ± 0.01

About 10 μCi of each ligand in a saline solution was injected. For in vivo blocking study, anastrozole (2 mg/kg) was injected at 2 min prior to the injection of radiotracers. Rats were sacrificed at 60 min post-injection, organs of interest were removed and weighed, and the radioactivity was counted. Data shown are the mean ± SD of three rats..

Pharmacological specificity of [^{125}I]5 binding in vivo. Effects of the pre-treatment with various compounds on stomach and ovary distribution of [^{125}I]**5** were examined to assess the in vivo pharmacological specificity. Specific binding of [^{125}I]**5** in the stomach and ovaries were significantly reduced by pre-treatment with selective aromatase inhibitors, anastrozole, letrozole, and YM511 (Figure 2A, $P < 0.05$), suggesting a potent in vivo competitive binding of these compounds with [^{125}I]**5** for aromatase. However, exemestane which is an steroidal aromatase inhibitor showed no effect on the specific binding of [^{125}I]**5** (Figure 2A). Furthermore, an in vivo competition of [^{125}I]**5** binding with anastrozole (dose range 0.0001 mg/kg - 2 mg/kg) was conducted. Anastrozole inhibited the specific bindings of [^{125}I]**5** dose-dependently, in both the stomach and ovaries (Figure 2B), thus indicating the binding of [^{125}I]**5** to aromatase was saturable.

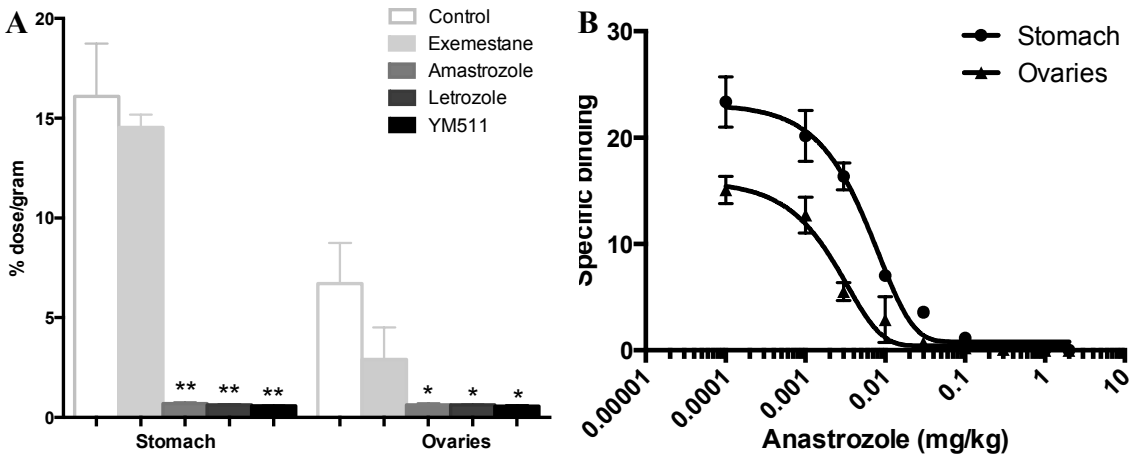

Figure 2. In vivo blockade on the uptake of [^{125}I]**5** in stomach and ovaries of female rats. **A**. Various drugs with a dose of 2 mg/kg was injected at 2 min prior to the injection of 10 μCi [^{125}I]**5.** Rats were sacrificed at 60 min after the injection of [^{125}I]**5**. The stomach and ovaries were removed and counted. The % dose/g uptakes in the stomach and ovaries were compared between saline-pretreated (control) and drug-pretreated rats. Data shown are the mean ± SD of three rats.

B. Anastrozole (dose range 0.0001 mg/kg – 2 mg/kg) was injected at 2 min prior to the injection of [^{125}I]**5** (10 μCi). Rats were sacrificed at 60 min after the injection of [^{125}I]**5**. The stomach and ovaries were removed and counted. The % dose/g uptakes in the stomach and ovaries of rats under treatment of the highest dose of anastrozole (2 mg/kg) were used as the background and the specific binding was calculated as the ratios of uptake value/background on a % dose/g basis. Data shown are the mean ± SEM of three rats.

Ex vivo autoradiography of [^{125}I]5 and [^{125}I]11. At 60 min post-injection of [^{125}I]**5** and [^{125}I]**11,** autoradiograms of sections from rat stomach and ovaries showed strong binding which was completely blocked in the presence of anastrozole (2 mg/kg, injected

at 2 min prior to the injection of [^{125}I]**5** and [^{125}I]**11**, Figure 3A, B). However, the addition of anastrozole did not show any effect on the binding of [^{125}I]**5** and [^{125}I]**11** in the adrenal glands (Figure 3C). The autoradiograms of brain sections showed intense labeling by [^{125}I]**5** in the amygdala and the bed nucleus of the stria terminalis (BNST), areas known to have high densities of aromatase. In rats pretreated with anastrozole (2 mg/kg, injected at 2 min prior to the injection of [^{125}I]**5**), the binding signals were significantly reduced compared to the matched sections of the control rats (Figure 3D). The regional distribution observed with [^{125}I]**5** was consistent with those reported for other aromatase ligands.[15, 17] [^{125}I]**11** was also detected in the BNST and the amygdala of male rats, while [^{125}I]**11** displayed a weak signal, compared with [^{125}I]**5** (Figure 3E). Similar as [^{125}I]**5** and [^{125}I]**11,** autoradiograms of sections from rat stomach and ovaries also showed strong binding at 60 min post-injection of [^{125}I]**8**. The binding signal was completely blocked in the presence of anastrozole. However, the autoradiograms of brain sections failed to show any labeling by [^{125}I]**8** (data not shown).

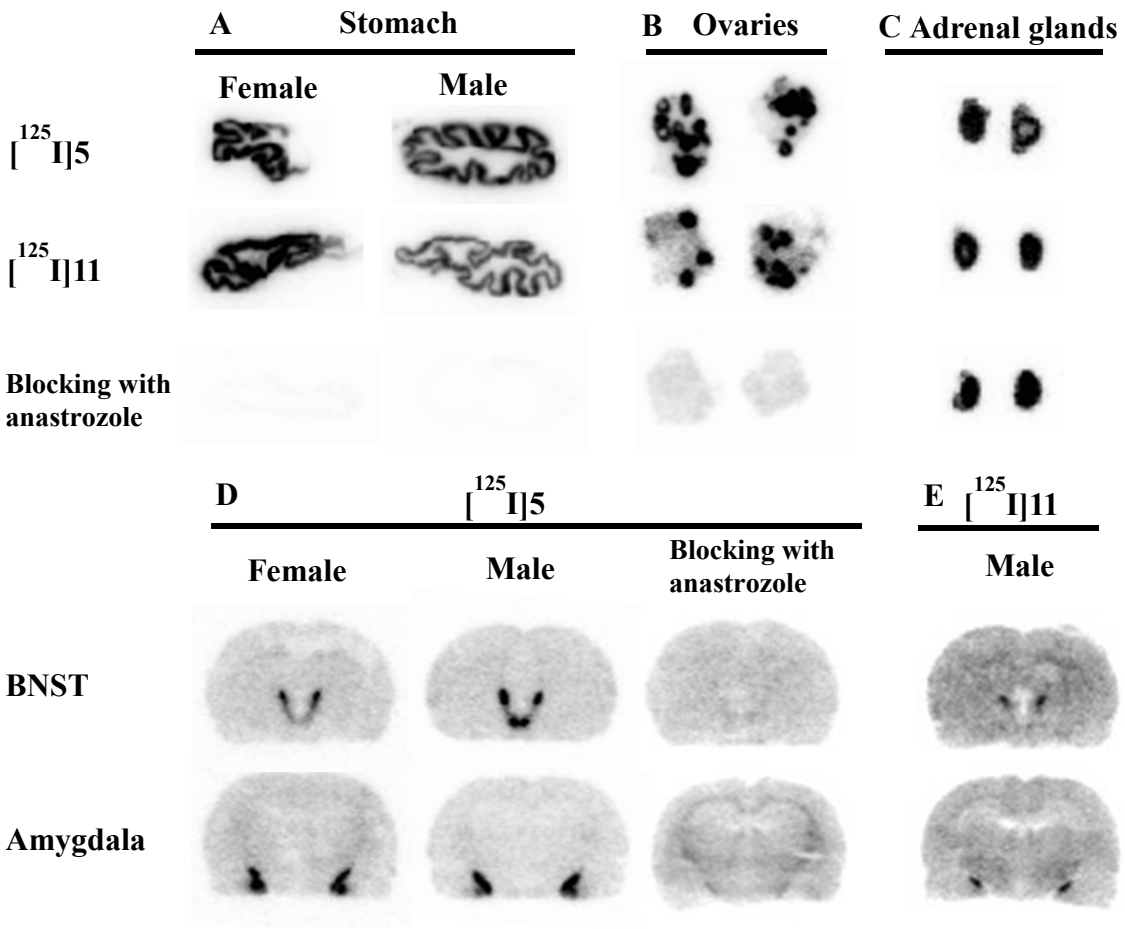

Figure 3. Ex vivo autoradiograms of [^{125}I]**5** and [^{125}I]**11** in rats at 60 min post iv injection. High levels of radioactivity were observed in stomach (**A**) and ovaries (**B**) sections. The high regional uptakes in BNST and amygdala were also observed in brain sections (**D, E**). The bindings in stomach, ovaries and brain were blocked in the presence of anastrozole (2 mg/kg, injected at 2 min prior to the injection of [^{125}I]**5** and [^{125}I]**11**). High non-specific binding was observed in adrenal glands (**C**). BNST: bed nucleus of stria terminalis.

X-ray crystal structures of 5 and 11. X-ray crystal structures of **5** and **11** were obtained in order to gain reliable structural information which is needed for molecular docking calculations. A crystal of **5** was grown slowly from a mixture of methanol/THF

and ethyl acetate (EtOAc). The size of the crystal used for structure determination was 0.25 × 0.22 × 0.2 mm, whereas the size of the crystal for **11** was 0.28 × 0.21 × 0.1 mm (grown from methanol/THF/EtOAc). The crystal for **5** showed the space group P $2_12_12_1$ (orthorhombic) whereas **11** crystallyzed in $P2_1$ (monoclinic) (Figure 4). Both compounds **5** and **11** have two crystallographically-independent structures with 50% probability each. ORTEP drawings of one of the two independent structures for **5** and **11** are shown in Figure 4.

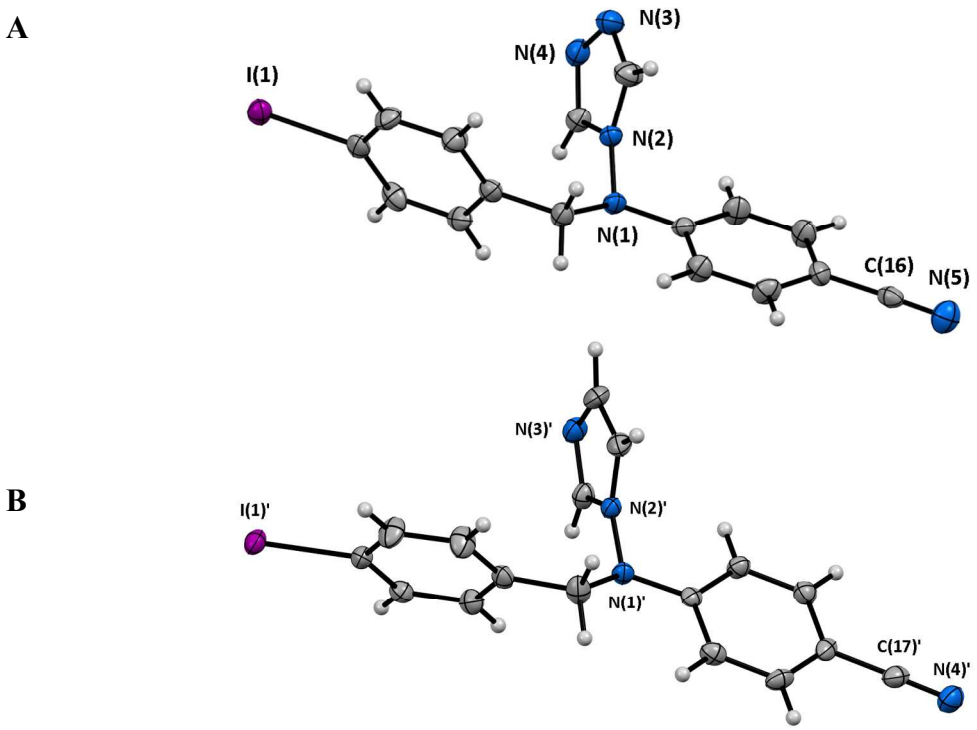

Figure 4: ORTEP drawing of **5** (A) and **11** (B) of the asymmetric unit with 50% thermal ellipsoids.

Molecular docking study of interactions between 5, 11, and human aromatase. Docking of compounds **5** and **11** to the aromatase enzyme was performed to investigate their binding modes. The binding of both compounds displayed similar π-π stacking and interactions of their benzyl rings with residues of aromatase; Ile 133, Phe 134, Phe 221,

Thr 224, Ala 306, Thr 310, Val 370, Leu 372, Leu 477 (Figure 5). Compound **5** formed a hydrogen bond between the second nitrogen of its triazole ring and Ser 478, the latter of which plays an important role in anti-aromatase activity when androstenedione is a natural substrate.[28] The amino acid forms hydrogen bonds through a water-mediated network, initiating enolization of the aromatase and the C3-keto oxygen of androstenedione.[28] Additional studies identified that Ser 478 is an important target to achieve selectivity of aromatase inhibition.[29-32] Interactions between compound **5** and Ser 478 may partially contribute to the observed aromatase inhibition. The atomic structures of compound **5** and **11** share some similarities, including the presence of a heterocyclic triazole and imidazole ring system, which differ in the presence of either a carbon or nitrogen in the ring. Both compounds may bind similarly to aromatase via hydrophobic interactions with Ser 478, and through hydrogen-bond interactions between the shared nitrogen facing the residue of the triazole/imidazole moieties with a water molecule. This water molecule also forms a hydrogen-bond bridge with both the hydroxyl of Ser 478 and another water molecule that coordinates to the catalytic site Fe^{2+} on the heme group of aromatase, similar to the proposed binding modes of Verdenafil and Sildenafil to PDE5.[33] This proposed interaction fits well with the comparable IC_{50} values of two compounds observed in a binding assay with human aromatase (CYP19) since these compounds bind in a similar fashion even in the absence of a direct hydrogen-bond interaction with Ser 478. Other binding modes were observed outside the active site of aromatase (data not shown). Previous studies mention possible steric interactions when docking azole fungicides into the active site of aromatase.[34] It is possible that both compounds **5** and **11** bind at an away site, inducing allosteric changes at the active site and inhibiting

aromatase from binding to androstenedione as observed in higher energy binding modes. More details are provided in the supplementary information.

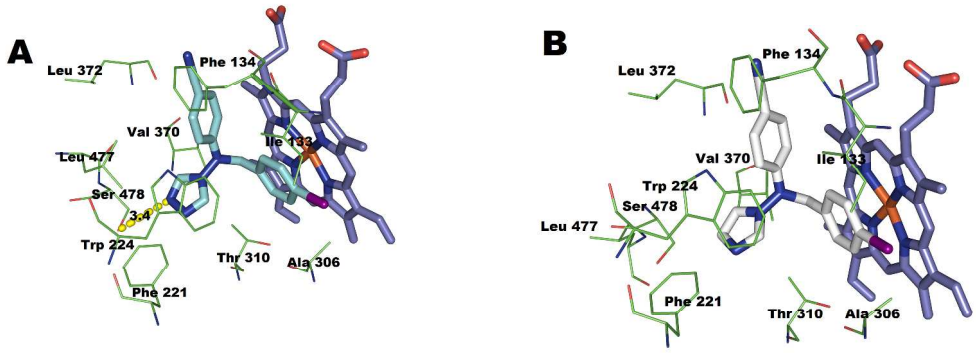

Figure 5. Molecular docking poses of compound **5** represented in cyan (A) and **11** represented in white (B) in aromatase's active site (PDB ID: 4KQ8)[51]; yellow dash line indicates a possible hydrogen bond formed between Ser 478 and triazole nitrogen of compound **5**.

Discussion and conclusions

The present study showed that [^{125}I]**5,** [^{125}I]**8,** and [^{125}I]**11** had an abundant accumulation in rat stomach, which was completely blocked in the presence of aromatase inhibitors. Our result is consistent with a study by Ozawa et al. in which they showed the presence of gastric aromatase in parietal cells using [^{11}C]vorozole.[15] In addition, for the first time, we found that the uptake of [^{125}I]**5** in females was significantly higher than in males. The underlying mechanisms responsible for high accumulation of aromatase tracers in stomach as well as gender difference still unclear. It probably related to

ghrelin's function and energy metabolism. As is known to all, ghrelin is an important hormone regulating energy metabolism what shows significant gender difference. It has been reported that the aromatase mRNA-expressing cells and ghrelin immuno-positive cells are localized close to each other in stomach of female and male rats, and that estrogen treatment can induce ghrelin mRNA expression and peptide production in isolated stomach cells.[35] Another human study showed estrogen replacement therapy increased human plasma ghrelin levels, and according to clinical statistics, women have higher plasma ghrelin levels than men.[36, 37] Since evidence showed estrogen treatment induced ghrelin releasing in isolated stomach cells, gastric aromatase, which also showed a significant gender difference, may play an important role in regulating ghrelin, further affected energy metabolism.

Our present study also showed a high accumulation of [^{125}I]**5** in rat ovaries, which is expected as the ovaries are the main site of peripheral estrogen production. The standard deviation was large because the female rats used in the present study are in random stages of the estrus cycle. Ovarian aromatase expression, [^{11}C]vorozole binding, and enzymatic activity are reported to be strongly dependent on the stage of the estrus cycle.[38, 39] According to another study by Kobayashi et al., the protein and mRNA levels of ovary aromatase significantly decrease during estrus and diestrus of female rats while stomach aromatase remained unchanged.[40] These studies suggest that gastric aromatase is not significantly related to the estrus cycle.

The autoradiograms of the brain showed a high specific binding of [^{125}I]**5** in the BNST and amygdala. The present data agree with an earlier report by Takahashi et al. using [^{11}C]vorozole.[17] These regions are also reported by other researchers to show high

aromatase activity,[5] high levels of aromatase mRNA,[41, 42] and immunoactivity[43, 44] in rat brain. Aromatase immunoreactive neurons have also been detected in the hypothalamic area of rat brain,[45] however, we failed to observe any specific binding of our compounds in the hypothalamus in the present study. This may be due to the varying sensitivities between the different techniques. Moreover, the aromatase-rich areas detected by [^{11}C]vorozole varies slightly among rodents, non-human primates and humans.[14, 17, 18] While there were no significant differences in aromatase expression between gender or gonadal/hormonal conditions in rat brain,[42] the sex differences of specific binding patterns in rat brain requires further study.

Aromatase has been reported as overexpressed and implicated in women diagnosed with breast cancer,[6] endometriosis,[46] brain, lung, and hepatic cancer.[8, 47, 48] Moreover, aromatase is also reported to be linked to brain disorders including Alzheimer's disease[10] and autism.[49] Although current studies on aromatase imaging are still restricted to expression and physiological function of aromatase, the radiotracers described here might be developed as potential radiopharmaceuticals for the diagnosis and clinical assessment of aromatase-related diseases.

In summary, several radioiodinated agents targeting aromatase have been prepared and evaluated. Of these, [^{125}I]**5** and [^{125}I]**11** are useful tools for aromatase studies in peripheral organs and [^{125}I]**5** is also a good tool for brain aromatase study. When labeled with ^{123}I, [^{123}I]**5** may be a good SPECT agent for brain aromatase imaging studies. Further characterization of these new ligands for human aromatase imaging studies is currently ongoing in our laboratory.

Experimental section

1 General

1.1 All reagents and solvents were purchased from commercial sources (Aldrich, Acros, or Alfa Inc.) and used without further purification, unless otherwise indicated. Solvents were dried through a molecular sieve system (Pure Solve Solvent Purification System; Innovative Technology, Inc.). ^{1}H spectra and ^{13}C NMR were recorded on an Avance spectrometer at 400 MHz and 100 MHz, respectively, and referenced to NMR solvents as indicated. Chemical shifts are reported in units of ppm (δ), with a coupling constant, *J*, in Hz. Multiplicity is defined by singlet (s), doublet (d), triplet (t), broad (br), and multiplet (m). High-resolution mass spectrometry (HRMS) data was obtained with an Agilent (Santa Clara, CA) G3250AA LC/MSD TOF system. Thin-layer chromatography (TLC) analyses were performed using Merck (Darmstadt, Germany) silica gel 60 F_{254} plates. Generally, crude compounds were purified by flash column chromatography (FC) packed with silica gel (Aldrich). HPLC was performed on an Agilent 1100 series system. Two HPLC conditions were used to test the purity of the final compounds. All compounds showed a purity > 95%. A Cobra II auto-gamma counter (Perkin-Elmer) measured ^{125}I radioactivity. Reactions of non-radioactive chemical compounds were monitored by TLC analysis with pre-coated plates of silica gel 60 F_{254}. Solid-phase extraction cartridges (SEP Pak® Light QMA, Oasis® HLB 3cc) were obtained from Waters (Milford, MA, USA).

1.2 Animals. Male and female Spague-Dawley rats weighing 220-250 g were used in biodistribution and ex vivo autoradiography studies. The rats were housed in an animal facility with 12 hr light and dark cycles with access to food and water freely. All animal experiments were carried out according to the ethics and animal welfare regulation

requirements approved by the Institutional Animal Care and Use Committee (University of Pennsylvania).

2 Synthesis of 4-Benzyl(4H-1,2,4-triazol-4-yl)amino)benzonitrile derivatives

2.1 4-((4H-1,2,4-triazol-4-yl)amino)benzonitrile and 4-((4-bromobenzyl)(4H-1,2,4-triazol-4-yl)amino)benzonitrile (1a). 4-((4H-1,2,4-triazol-4-yl)amino)benzonitrile and 4-((4-bromobenzyl)(4H-1,2,4-triazol-4-yl)amino)benzonitrile (**1a**) were synthesized according to the published report by Wanatanabe et al.[23] as summarized in Scheme 1.

2.2 4-((4-Fluorobenzyl)(4H-1,2,4-triazol-4-yl)amino)benzonitrile (1b). To a stirred solution of 4-((4*H*-1,2,4-triazol-4-yl)amino)benzonitrile (100 mg, 0.54 mmol) in DMF (10 mL) at room temperature, K_2CO_3 (82 mg, 0.59 mmol) and 1-(bromomethyl)-4-fluorobenzene (111 mg, 0.59 mmol) were added. After maintaining the mixture at room temperature for 2 h, it was then extracted with EtOAc. The combined organic layers were dried over $MgSO_4$, filtered, and concentrated in vacuo to afford a crude product. Purification by FC (EtOAc/Hexanes, 50/50, V/V) afforded **1b** (134 mg, 85.4%) as white solid. ^{1}H NMR (400 MHz, $CDCl_3$) δ: 8.11(s, 2H), 7.52 (dd, J = 2.0, 2.4 Hz, 2H), 7.16 (dd, J = 5.2, 5.2 Hz, 2H), 6.97 (t, J = 8.4 Hz, 2H), 6.64 (dd, J = 2.0, 2.0 Hz, 1H), 4.85 (s, 2H). ^{13}C NMR (100 MHz, $CDCl_3$) δ: 164.08, 162.42, 150.49, 142.64, 133.98, 130.12, 130.04, 129.43, 129.40, 118.45, 116.37, 116.16, 113.60, 105.11, 57.42. HRMS calcd for; $C_{16}H_{12}FN_5$ 293.1077 found, 294.1117 $[M+H]^+$.

2.3 4-((4-Methoxybenzyl)(4H-1,2,4-triazol-4-yl)amino)benzonitrile (1b). To a stirred solution of 4-((4*H*-1,2,4-triazol-4-yl)amino)benzonitrile (100 mg, 0.54 mmol) in dimethylformamide (DMF) (10 mL) at room temperature, K_2CO_3 (82 mg, 0.59 mmol)

and 1-(bromomethyl)-4-methoxybenzene (117 mg, 0.59 mmol) were added. After maintaining the mixture at room temperature for 2 h, it was then extracted with EtOAc. The combined organic layers were dried over $MgSO_4$, filtered, and concentrated in vacuo to afford a crude product. Purification by FC (EtOAc/Hexanes, 50/50, V/V) afforded **1c** (142 mg, 86.6%) as a white solid. ^{1}H NMR (400 MHz, $CDCl_3$) δ: 8.05 (s, 2H), 7.98 (s, 2H), 7.55 (d, *J* = 9.2Hz, 2H), 7.07 (d, *J* = 8.8 Hz, 2H), 6.82 (d, *J* = 8.8 Hz, 2H), 6.98 (d, *J* = 8.8 Hz, 2H), 4.81 (s, 2H), 3.76 (s, 3H). ^{13}C NMR (100 MHz, $CDCl_3$) δ: 150.56, 142.70, 134.01, 129.74, 125.20, 118.55, 114.65, 113.52, 104.92, 57.51, 55.27. HRMS calcd for: $C_{17}H_{15}N_5O$ 305.1277; found, 306.1282 $[M+H]^+$.

2.4 4-(((6-Bromopyridin-3-yl)methyl)(4H-1,2,4-triazol-4-yl)amino)benzonitrile (1d). To a stirred solution of 4-((4*H*-1,2,4-triazol-4-yl)amino)benzonitrile (100 mg, 0.54 mmol) in DMF (10 mL) at room temperature, K_2CO_3 (82 mg, 0.59 mmol) and 2-bromo-5-(bromomethyl)pyridine (146 mg, 0.59 mmol) were added. After maintaining at room temperature for 2 h, the mixture was extracted with EtOAc. The combined organic layers were dried over $MgSO_4$, filtered, and concentrated in vacuo to afford a crude product. Purification by FC (EtOAc/Hexanes, 50/50, V/V) afforded **1d** (160 mg, 84.1%) as a white solid. ^{1}H NMR (400 MHz, $CDCl_3$) δ: 8.35 (d, *J* = 2.4 Hz, 1H), 8.21 (s, 2H), 7.64 (dd, *J* = 2.0, 2.0 Hz, 2H), 7.52 (d, *J* = 8.0 Hz, 1H), 7.40 (dd, *J* = 2.0, 2.0 Hz, 1H), 6.70 (d, *J* = 9.2 Hz, 1H), 4.91 (s, 2H). ^{13}C NMR (100 MHz, $CDCl_3$) δ: 149.94, 149.65, 143.26, 142.27, 137.85, 134.27, 128.78, 128.60, 118.10, 113.84, 106.40, 55.59. HRMS calcd for $C_{15}H_{11}BrN_6$ 354.0229; found, 355.0231 $[M+H]^+$.

2.5 4-((4H-1,2,4-triazol-4-yl)(4-(tributylstannyl)benzyl)amino)benzonitrile (4). Compound **1a** (100 mg, 0.28 mmol) and bis(tributyltin) (820 mg, 1.42 mmol) were

dissolved in toluene (10 mL), and tetrakis(triphenylphosphine)palladium(0) (60 mg, 0.05 mmol) was added. The mixture was refluxed under argon for 2 h and condensed under reduced pressure. The residue was then applied to FC (hexanes/EtOAc 3:1), which afforded **4** (59 mg, 37.6%) as a colorless oil. ^{1}H NMR (400 MHz, $CDCl_3$) δ: 8.13 (s, 2H), 7.56 (d, *J* = 9.2 Hz, 2H), 7.44 (d, *J* = 8.0 Hz, 2H), 7.15 (d, *J* = 8.0 Hz, 2H), 6.66 (d, *J* = 9.2 Hz, 2H), 4.95 (s, 2H), 1.56-1.52 (m, 6H), 1.51-1.48 (m, 7H), 1.36-1.27 (m, 5H), 0.91-0.87 (m, 9H). ^{13}C NMR (100 MHz, $CDCl_3$) δ: 150.55, 143.72, 142.70, 137.31, 134.05, 133.13, 127.54, 127.34, 118.59, 113.27, 109.83, 58.28, 29.01, 27.28, 13.64, 9.63. HRMS calcd for $C_{28}H_{39}N_5Sn$ 565.2227; found, 566.2382 $[M+H]^+$.

2.6 4-((4-Iodobenzyl)(4H-1,2,4-triazol-4-yl)amino)benzonitrile (5). Compound **4** (30 mg, 0.053 mmol) and I_2 (28 mg, 0.11 mmol) were dissolved in dichloromethane (DCM) (15 mL), and the reaction mixture was stirred at room temperature for a half hour. Then, 2M $Na_2S_2O_3$ was added, DCM was extracted, the reaction mixture was condensed, and the crude product was purified by flash column to afford **5** as a white solid (20 mg, 95.6%). ^{1}H NMR (400 MHz, $CDCl_3$) δ: 8.43 (s, 2H), 7.67 (d, *J* = 8.4 Hz, 2H), 7.61 (d, *J* = 9.2 Hz, 2H), 7.05 (d, *J* = 8.1 Hz, 2H), 6.75 (d, *J* = 9.2 Hz, 2H), 4.95 (s, 2H). ^{13}C NMR (100 MHz, $CDCl_3$) δ: 150.80, 143.17, 138.21, 133.95, 133.68, 130.13, 118.47, 113.91, 104.88, 94.28, 57.60. HRMS calcd for $C_{16}H_{12}IN_5$; found, 402.0209 $[M+H]^+$.

2.7 4-((4-Hydroxybenzyl)(4H-1,2,4-triazol-4-yl)amino)benzonitrile (2). A solution of **1c** (100 mg, 0.33 mmol) and 1M BBr_3 (1 mL) was dissolved in DCM (15 mL), and the reaction was stirred at -78 °C for 15 min. The solution was then stirred at room temperature for 1 h, and CH_3OH (10 mL) was added. The reaction was purified by FC, which afforded **2** as a white solid (57 mg, 60.1%). ^{1}H NMR (400 MHz, $CDCl_3$) δ: 8.47 (s,

2H), 7.70 (d, J = 9.2 Hz, 2H), 7.18 (d, J = 8.8 Hz, 2H), 6.87 (d, J = 8.8 Hz, 2H), 6.80 (d, J = 8.4 Hz, 2H), 5.02 (s, 2H). ^{13}C NMR (100 MHz, $CDCl_3$) δ: 151.72, 142.86, 133.70, 130.19, 125.25, 118.53, 115.52, 113.94, 113.82, 103.86, 56.98, 56.27. HRMS calcd for $C_{16}H_{13}N_5O$ 291.1120; found, 292.1122 $[M+H]^+$.

2.8 4-((4-(2-Fluoroethoxy)benzyl)(4H-1,2,4-triazol-4-yl)amino)benzonitrile (3a). To a stirred solution of **2** (100 mg, 0.34 mmol) in DMF (10 mL) at room temperature, K_2CO_3 (95 mg, 0.68 mmol) and 1-bromo-2-fluoro-ethane (48 mg, 0.38 mmol) were added. After maintaining at room temperature for 2 h, the mixture was then extracted with EtOAc. The combined organic layers were dried over $MgSO_4$, filtered, and concentrated in vacuo to afford a crude product. Purification by FC (EtOAc/hexanes, 50/50, V/V) yielded **3a** (99 mg, 86.3%) as a yellow solid. ^{1}H NMR (400 MHz, $CDCl_3$) δ: 8.07 (d, J = 2.8Hz, 2H), 8.02 (s, 1H), 7.59 (dd, J = 2.4, 2.0 Hz, 2H), 7.11 (dd, J = 2.0, 2.0 Hz, 2H), 6.70 (dd, J = 2.0, 2.4 Hz, 2H), 4.83-4.80 (m, 3H), 4.70 (t, J = 4.0 Hz, 1H), 4.23 (t, J = 4.0 Hz, 1H), 4.16 (t, J = 4.0 Hz, 1H). ^{13}C NMR (100 MHz, $CDCl_3$) δ: 150.48, 142.65, 134.07, 129.81, 125.85, 118.50, 115.38, 113.52, 105.15, 82.57, 80.87, 67.27, 67.06, 57.55. HRMS calcd. for $C_{18}H_{16}FN_5O$ 337.1339; found, 338.1419 $[M+H]^+$.

2.9 4-((4-(3-Fluoropropoxy)benzyl)(4H-1,2,4-triazol-4-yl)amino)benzonitrile (3b). To a stirred solution of **2** (100 mg, 0.34 mmol) in DMF (10 mL) at room temperature, K_2CO_3 (95 mg, 0.68 mmol) and 3-fluoropropyl 4-methylbenzenesulfonate (88 mg, 0.38 mmol) were added. After maintaining at room temperature for 2 h, the mixture was extracted with EtOAc. The combined organic layers were then dried over $MgSO_4$, filtered, and concentrated in vacuo to give a crude product. Purification by FC (EtOAc/hexanes, 50/50, V/V) yielded **3b** (102 mg, 85.9%) as a yellow solid. ^{1}H NMR (400 MHz, $CDCl_3$)

δ: 8.07 (s, 2H), 7.61 (d, *J* = 8.8, 2H), 7.10 (d, *J* = 8.4 Hz, 2H), 6.87 (d, *J* = 8.8Hz, 2H), 6.71 (d, *J* = 8.8Hz, 2H), 4.83 (s, 2H), 4.72 (t, *J* = 4.0 Hz, 1H), 4.60 (t, *J* = 4.0 Hz, 1H), 4.15-4.08 (m, 2H), 2.25-2.14 (m, 2H). ^{13}C NMR (100 MHz, $CDCl_3$) δ: 159.42, 150.47, 142.66, 134.09, 129.76, 125.30, 118.49, 115.26, 113.50, 105.18, 81.36, 79.72, 63.66, 63.61, 57.59, 30.42, 30.23. HRMS calcd for; $C_{19}H_{18}FN_5O$ 351.1495 found, 352.1509 $[M+H]^+$.

***3* Synthesis of 4-((4-iodobenzyl)(pyrimidin-5-yl)amino)benzonitrile**

3.1 4-(Pyrimidin-5-ylamino)benzonitrile and 4-((4-bromobenzyl)(pyrimidin-5-yl) amino)benzonitrile (6a). 4-(pyrimidin-5-ylamino)benzonitrile and 4-((4-bromobenzyl)(pyrimidin-5-yl)amino) benzonitrile (**6a**) were prepared according to the published reported by Okada et al.[50] as summarized in Scheme 2.

3.2 4-(((6-Bromopyridin-3-yl)methyl)(pyrimidin-5-yl)amino)benzonitrile (6b). To a stirred solution of 4-(pyrimidin-5-ylamino)benzonitrile (100 mg, 0.51 mmol) in DMF (10 mL) at room temperature, K_2CO_3 (141 mg, 1 mmol) and 2-bromo-5-(bromomethyl)pyridine (139 mg, 0.56 mmol) were added. After maintaining at room temperature for 2 h, the mixture was then extracted with EtOAc. The combined organic layers were dried over $MgSO_4$, filtered, and concentrated in vacuo to afford a crude product. Purification by FC (EtOAc/hexanes, 50/50, V/V) yielded **6b** (151 mg, 81.3%) as a white solid. ^{1}H NMR (400 MHz, $CDCl_3$) δ: 9.03 (s, 1H), 8.67 (s, 2H), 8.63 (s, 2H), 8.33 (t, *J* = 0.8 Hz, 1H), 7.56 (d, *J* = 8.8 Hz, 2H), 7.48 (t, *J* = 0.8 Hz, 2H), 6.96 (d, *J* = 8.8 Hz, 2H), 5.02 (s, 2H). ^{13}C NMR (100 MHz, $CDCl_3$) δ: 154.74, 152.24, 149.32, 148.58, 148.23, 141.91, 140.61, 136.66, 134.10, 131.12, 128.54, 118.66, 117.63, 115.93, 104.91, 53.12. HRMS calcd for $C_{17}H_{12}BrN_5$ 365.0276; found, 366.0420 $[M+H]^+$.

3.3 4-(Pyrimidin-5-yl(4-(tributylstannyl)benzyl)amino)benzonitrile (7). Compound **6a** (100 mg, 0.27 mmol) and bis(tributyltin) (820 mg, 1.42 mmol) were dissolved in toluene (10 mL), and tetrakis(triphenylphosphine)palladium(0) (60 mg, 0.05 mmol) was subsequently added. The mixture was refluxed under argon for 2 h and condensed under reduced pressure. The resulting residue was applied to FC (hexanes/EtOAc 3:1) which afforded **7** (65 mg, 41.3%) as a colorless oil. ^{1}H NMR (400 MHz, $CDCl_3$) δ: 8.99 (s, 1H), 8.67 (s, 2H), 7.73 (d, *J* = 6.0 Hz, 2H), 7.53 (d, *J* = 8.8 Hz, 2H), 7.45 (d, *J* = 8.0 Hz, 2H), 7.40 (d, *J* = 7.6 Hz, 2H), 7.22 (d, *J* = 7.6 Hz, 2H), 7.16 (d, *J* = 8.8 Hz, 2H), 5.04 (s, 2H), 1.58-1.52 (m, 5H), 1.36-1.28 (m, 7H), 1.08-1.04 (m, 5H), 0.91-0.87 (m, 9H). ^{13}C NMR (100 MHz, $CDCl_3$) δ: 154.17, 152.22, 150.04, 142.03, 137.17, 133.87, 130.36, 127.92, 127.87, 125.81, 119.09, 117.37, 103.88, 55.93, 29.04, 27.33, 13.64, 9.61. HRMS calcd for; $C_{30}H_{40}N_4Sn$ 576.2275 found, 577.2451 $[M+H]^+$.

3.4 4-((4-Iodobenzyl)(pyrimidin-5-yl)amino)benzonitrile (8). A solution of **7** (30 mg, 0.052 mmol) and I_2 (28 mg, 0.11 mmol) dissolved in DCM (15 mL) was stirred at room temperature for a half hour before 20 mL 2M $Na_2S_2O_3$ was added. DCM was then extracted, the reaction mixture was condensed, and the crude product was purified by FC to afford **8** as a white solid (20 mg, 94.2%). ^{1}H NMR (400 MHz, $CDCl_3$) δ: 9.01 (s, 1H), 8.65 (s, 2H), 7.70 (dd, *J* = 2.0, 0.8 Hz, 2H), 7.55 (dd, *J* = 2.0, 2.0 Hz, 2H), 7.02 (d, *J* = 8.8 Hz, 2H), 7.55 (dd, *J* = 2.4, 2.0 Hz, 2H), 4.99 (s, 2H). ^{13}C NMR (100 MHz, $CDCl_3$) δ: 154.42, 152.17, 149.68, 140.82, 138.31, 135.69, 133.96, 128.88, 117.45, 105.11, 93.30, 55.53. HRMS calcd for; $C_{18}H_{13}IN_4$ 412.0185 found, 413.0212 $[M+H]^+$.

4 Synthesis of 4-((1H-imidazol-1-yl)(4-iodobenzyl)amino)benzonitrile

4.1 4-((4-Bromobenzyl)(1H-imidazol-1-yl)amino)benzonitrile (9). 4-((4-bromobenzyl)(1*H*-imidazol-1-yl)amino)benzonitrile (**9**) was prepared according to the published report by Adje et al.[25]

4.2 4-((1H-imidazol-1-yl)(4-(tributylstannyl)benzyl)amino)benzonitrile (10). To a solution of **9** (100 mg, 0.28 mmol) and bis(tributyltin) (820 mg, 1.42 mmol) dissolved in toluene (10 mL), tetrakis(triphenylphosphine)palladium(0) (60 mg, 0.05 mmol) was added. The mixture was refluxed under argon for 2 h and condensed under reduced pressure. The residue was applied to FC (hexanes/EtOAc 3:1) which afforded **10** (53 mg, 32.9%) as a colorless oil. ^{1}H NMR (400 MHz, $CDCl_3$) δ: 7.54-7.46 (m, 5H), 7.21 (d, *J* = 8.0 Hz, 2H), 7.14 (t, *J* = 1.2 Hz, 1H), 6.93 (t, *J* = 1.2 Hz, 1H), 6.58 (d, *J* = 9.2 Hz, 2H), 4.89 (s, 2H), 1.56-1.52 (m, 5H), 1.36-1.25 (m, 7H), 0.95-0.92 (m, 5H), 0.91-0.87 (m, 9H). ^{13}C NMR (100 MHz, $CDCl_3$) δ: 151.46, 142.79, 137.08, 136.92, 134.28, 133.80, 129.08, 126.99, 119.04, 118.57, 112.81, 103,57, 60.37, 58.26, 29.04, 27.31, 14.19, 9.61. HRMS calcd for $C_{29}H_{40}N_4Sn$ 564.2275; found, 565.3219 $[M+H]^+$.

4.3 4-((1H-imidazol-1-yl)(4-iodobenzyl)amino)benzonitrile (11). Compound **10** (30 mg, 0.053 mmol) and I_2 (28 mg, 0.11mmol) were dissolved in DCM (15 mL). The reaction mixture was stirred at room temperature for a half hour, 2M $Na_2S_2O_3$ was added, DCM was extracted, the mixture was condensed, and the crude product was purified by FC to afford **11** as a white solid (20 mg, 92.9%). ^{1}H NMR (400 MHz, $CDCl_3$) δ: 7.70 (d, *J* = 8.4 Hz, 2H), 7.54 (d, *J* = 8.8 Hz, 2H), 7.46 (s, 1H), 7.15 (d, *J* = 1.2 Hz, 1H), 7.02 (d, *J* = 8.4 Hz, 2H), 6.93 (t, *J* = 1.2 Hz, 2H), 6.58 (d, *J* = 9.2 Hz, 2H), 4.84 (s, 2H). ^{13}C NMR (100 MHz, $CDCl_3$) δ: 151.24, 138.24, 136.85, 134.31, 133.88, 129.53, 129.38, 118.86, 118.32,

113.07, 104.18, 94.21, 57.79. HRMS calcd. for $C_{17}H_{13}IN_4$ 400.0185; found, 401.0219 $[M+H]^+$.

5 In vitro binding assays using human CYP19 (aromatase). Binding assays were performed in glass tubes (12 × 75 mm) in a final volume of 250 μL. Competition experiments were performed in phosphate buffered saline (pH = 7.4) using [^{125}I]**5,** and 10^{-11}-10^{-6} M of competing drugs. Nonspecific binding was defined with 7 μM letrozole. Incubation was carried out for 60 min at room temperature and then terminated by separating bound from free radioligand by filtration through filter papers (FP-100, Brandel, MD). The filter papers were washed twice with ice-cold buffer (containing 20 mM Tris-HCl, pH = 7.4) and the radioactivity on the filter papers was counted in a gamma counter (Packard, D5003, Perkin Elmer, MA) with 70% efficiency. Human CYP19 (aromatase) was purchased from Corning Life Science (New York, United States). Competition experiments were analyzed using the GRG nonlinear curve-fitting program (Excel Solver) to obtain half-maximal inhibitory concentrations (IC_{50}) values.

6. Radiosynthesis of [^{125}I]5, [^{125}I]8 and [^{125}I]11. The radiolabeling of 4-((4-iodobenzyl)(4H-1,2,4-triazol-4-yl)amino)benzonitrile (**5**), 4-((4-iodobenzyl)(pyrimidin-5-yl)amino)benzonitrile **(8)** and 4-((1H-imidazol-1-yl)(4-iodobenzyl)amino)benzonitrile **(11)** were prepared by an iododestannylation reaction. The tin compounds, **4**, **7,** and **10** (100 μg in 100 μL of ethanol), I-125 sodium iodide, and 1N HCl (100 μL) were placed in sealed vials separately. 100 μL of H_2O_2 (3% in water) were added to this mixture via a syringe at room temperature. The iodination reaction was terminated after 10 min by adding 150 μL of saturated $NaHSO_3$ and the resulting solution was neutralized by the addition of

saturated $NaHCO_3$ solution. The mixture was passed through an activated C4 mini column, washed twice with 3 mL water, 3 mL 10% ethanolic solution, 3mL 20% ethanolic solution and the activity was eluted with 1 mL ethanol. HPLC purification was performed on a Phenomenex Gemini® 5 μm C18 250 mm × 4.6 mm column, with the following gradient and a flow rate of 1 mL/min: 0-15 min 10 mM ammonium formate buffer 90 to 0%, acetonitrile 10-100%; 15-20 min 100% acetonitrile. Radiochemical purities after HPLC purification for these ligands were >99%.

7. Partition coefficients. The partition coefficients were measured by mixing the appropriate radioligand (1 μCi) with 3 g each of 1-octanol and buffer (pH 7.4, 0.1 M phosphate) in a test tube. The test tube was then vortexed for 2 min and centrifuged for 10 min at room temperature. Two samples (2g each) from the 1-octanol and buffer layers were weighed and counted in a gamma counter. The partition coefficient was determined by calculating the ratio of counts per min/gram in octanol to that of the buffer. Samples of the 1-octanol layer were repartitioned until consistent partition coefficient values were obtained. The measurement was repeated three times.

8. In vivo biodistribution studies and block studies. Three rats per group were used for each biodistribution study. While under isofluorane anesthesia, 0.2 mL of a saline solution containing 10 μCi of radioactive tracer was injected into the femoral vein. The rats were sacrificed at the time indicated by cardiac excision while under anesthesia. Organs of interest were removed, weighed, and the radioactivity was counted in a gamma counter (Perkin Elmer, MA). The percent dose per organ and percent dose per gram were calculated by a comparison of the tissue counts to counts of 1% of the initial dose (100 times diluted aliquots of the injected material) measured simultaneously. In vivo

competitive binding of various compounds in the regional uptake of [^{125}I]**5** was investigated by pretreating animals with various competing drugs (2 mg/kg, each, iv injection at 2 min prior to injection of [^{125}I]**5**). The competing drugs were anastrozole, exemestane, letrozole, and YM511. The regional uptakes of stomach and ovaries in the drug-pretreated rats were compared to those of control rats pretreated with saline. In addition, various amounts of anastrozole (dose range 0.0001-2 mg/kg) were pre-injected 2 minutes prior to [^{125}I]**5)** to evaluate the in vivo saturability of [^{125}I]**5** binding to aromatase in stomach and ovaries.

9. Autoradiographic studies. For ex vivo autoradiographic studies, male and female Spague-Dawley rats (220-250 g) under anesthesia were intravenously injected with 0.5 mL of a saline solution containing 0.4-0.5 mCi of [^{125}I]**5** and [^{125}I]**11** respectively. At 60 min post-injection, the rats were sacrificed by cardiac excision while under anesthesia. The stomach, ovaries, adrenal glands, and brain were rapidly removed, placed in a Tissue-Tek OCT compound (Sakura, Japan), and frozen in a dry ice-acetone bath. After reaching equilibrium to -20 °C, 25 μm sections were consecutively cut by a cryostat microtome (Bright Instrument, Cambridgeshire, UK), thaw-mounted on gelatin-coated microscope slides, and air-dried at room temperature. The slides were then exposed to a phosphor screen (GE health care, Little Chalfont, UK) in an autoradiographic cassette for 2 h. The images were acquired through a Typhoon FLA 7000 (GE health care, Little Chalfont, UK). Blocking studies were carried out by pretreating the rats with anastrozole (2 mg/kg, i.v) prior to radioligand injection.

10. Molecular docking of interactions between Compound 5 and 11 with human aromatase. Molecular docking was performed to identify potential interactions between

the investigated compounds and the aromatase enzyme. Compounds **5** and **11** were generated as three dimensional pdb files using Chem3D Pro 14.0 software (CambridgeSoft). The crystal structure of recombinant human cytochrome P450 aromatase was obtained from Protein Data Bank (PDB ID: 4KQ8).[51] The protein structure was prepared by addition of hydrogen atoms by AutoDockTools-1.5.6 (Scripps Research Institute). Water molecules and androstenedione were removed from the structures and hydrogens were manually added using AutoDockTools-1.5.6 (Scripps Research Institute). All ligand bonds were identified as flexible. Docking experiments were performed using AutoDock Vina (Scripps Research Institute).[52]

Associated Content

Supporting Information: HPLC profiles of final compounds, X-ray crystallographic data for compound **5** and **11**, docking experiment supplied as Supporting Information. The crystallographic data have been deposited with the Cambridge Crystallographic Data Centre as CCDC 1473972 and 1473973 and are available free of charge on application to CCDC, 12 Union Road, Cambridge, CB2 1EZ, U.K. (fax, (+44)1223 336033; e-mail, deposit@ccdc.cam.ac.uk). **PDB ID Codes C5, C11:** Authors will release the atomic coordinates and experimental data upon article publication.

SMILES (CSV)

Corresponding author information

*Phone: (215) 662-3096. Fax: (215) 349-5035. E-mail: kunghf@gmail.com. Address: Hank F. Kung, Ph.D., 3700 Market Street, Suite 305, Department of Radiology, University of Pennsylvania School of Medicine, Philadelphia, PA 19104

Abbreviations Used

AI, aromatase inhibitor; BNST, the bed nucleus of stria terminalis; CNS, central nervous system; CYP 19, cytochrome P450, family 19; PET, positron emission tomography; SPECT, single-photon emission computed tomography; YM511, 4-[[(4-Bromophenyl)methyl]-4H-1,2,4-triazol-4-ylamino]benzonitrile.

Acknowledgement

Authors thank Trevor M. Penning, PhD, The Thelma Brown and Henry Charles Molinoff Professor of Pharmacology, Department of Systems Pharmacology and Translational Therapeutics and the Center for Excellence in Environmental Toxicology, Perelman

School of Medicine, University of Pennsylvania, for his suggestions on molecular modeling studies. We thank the Beijing Institute for Brain Disorders, Capital Medical University and the Department of Radiology, University of Pennsylvania for financial support.

References

1. Azcoitia, I.; Yague, J.; Garcia-Segura, L. M. Estradiol synthesis within the human brain. *Neuroscience* **2011,** *191*, 139-147.
2. Simpson, E. R.; Zhao, Y.; Agarwal, V. R.; Michael, M. D.; Bulun, S. E.; Hinshelwood, M. M.; Graham-Lorence, S.; Sun, T.; Fisher, C. R.; Qin, K. Aromatase expression in health and disease. *Recent Prog. Horm. Res.* **1996,** *52*, 185-213; discussion 213-214.
3. Leshin, M.; Baron, J.; George, F. W.; Wilson, J. D. Increased estrogen formation and aromatase activity in fibroblasts cultured from the skin of chickens with the Henny feathering trait. *J. Biol. Chem.* **1981,** *256*, 4341-4344.
4. Mahendroo, M. S.; Mendelson, C.; Simpson, E. Tissue-specific and hormonally controlled alternative promoters regulate aromatase cytochrome P450 gene expression in human adipose tissue. *J. Biol. Chem.* **1993,** *268*, 19463-19470.
5. Roselli, C. E.; Horton, L. E.; Resko, J. A. Distribution and Regulation of Aromatase Activity in the Rat Hypothalamus and Limbic System. *Endocrinology* **1985,** *117*, 2471-2477.
6. Bulun, S. E.; Simpson, E. R. Aromatase expression in women's cancers. In *Innovative Endocrinology of Cancer*, Berstein, L. M. S., R.J. , Ed. Springer: Berlin, 2008; pp 112-132.
7. Bulun, S. E.; Fang, Z.; Imir, G.; Gurates, B.; Tamura, M.; Yilmaz, B.; Langoi, D.; Amin, S.; Yang, S.; Deb, S. In *Aromatase and endometriosis*, Semin. Reprod. Med., 2004; 2004; pp 45-50.
8. Miceli, V.; Cervello, M.; Azzolina, A.; Montalto, G.; Calabrò, M.; Carruba, G. Aromatase and amphiregulin are correspondingly expressed in human liver cancer cells. *Ann. N. Y. Acad. Sci.* **2009,** *1155*, 252-256.
9. Garcia Segura, L. M. Aromatase in the brain: not just for reproduction anymore. *J. Neuroendocrinol.* **2008,** *20*, 705-712.
10. Ishunina, T. A.; van Beurden, D.; van der Meulen, G.; Unmehopa, U. A.; Hol, E. M.; Huitinga, I.; Swaab, D. F. Diminished aromatase immunoreactivity in the hypothalamus, but not in the basal forebrain nuclei in Alzheimer's disease. *Neurobiol. Aging* **2005,** *26*, 173-194.

11. Buzdar, A.; Howell, A. Advances in aromatase inhibition clinical efficacy and tolerability in the treatment of breast cancer. *Clin. Cancer Res.* **2001,** *7*, 2620-2635.
12. Cohen, M. H.; Johnson, J. R.; Li, N.; Chen, G.; Pazdur, R. Approval Summary Letrozole in the Treatment of Postmenopausal Women with Advanced Breast Cancer. *Clin. Cancer Res.* **2002,** *8*, 665-669.
13. Kil, K.-E.; Biegon, A.; Ding, Y.-S.; Fischer, A.; Ferrieri, R. A.; Kim, S. W.; Pareto, D.; Schueller, M. J.; Fowler, J. S. Synthesis and PET studies of [11 C-cyano] letrozole (Femara), an aromatase inhibitor drug. *Nucl. Med. Biol.* **2009,** *36*, 215-223.
14. Kim, S. W.; Biegon, A.; Katsamanis, Z. E.; Ehrlich, C. W.; Hooker, J. M.; Shea, C.; Muench, L.; Xu, Y.; King, P.; Carter, P. Reinvestigation of the synthesis and evaluation of [N-methyl-11 C] vorozole, a radiotracer targeting cytochrome P450 aromatase. *Nucl. Med. Biol.* **2009,** *36*, 323-334.
15. Ozawa, M.; Takahashi, K.; Akazawa, K.-h.; Takashima, T.; Nagata, H.; Doi, H.; Hosoya, T.; Wada, Y.; Cui, Y.; Kataoka, Y. PET of aromatase in gastric parietal cells using 11C-Vorozole. *J. Nucl. Med.* **2011,** *52*, 1964-1969.
16. Pareto, D.; Biegon, A.; Alexoff, D.; Carter, P.; Shea, C.; Muench, L.; Xu, Y.; Fowler, J. S.; Kim, S. W.; Logan, J. In Vivo Imaging of Brain Aromatase in Female Baboons:[11 C] Vorozole Kinetics and Effect of the Menstrual Cycle. *Mol. Imaging* **2013,** *12*, 518-524.
17. Takahashi, K.; Bergström, M.; Frändberg, P.; Vesström, E.-L.; Watanabe, Y.; Långström, B. Imaging of aromatase distribution in rat and rhesus monkey brains with [11 C] vorozole. *Nucl. Med. Biol.* **2006,** *33*, 599-605.
18. Biegon, A.; Kim, S. W.; Alexoff, D. L.; Jayne, M.; Carter, P.; Hubbard, B.; King, P.; Logan, J.; Muench, L.; Pareto, D. Unique distribution of aromatase in the human brain: In vivo studies with PET and [N‐methyl‐11C] vorozole. *Synapse* **2010,** *64*, 801-807.
19. Takahashi, K.; Hosoya, T.; Onoe, K.; Doi, H.; Nagata, H.; Hiramatsu, T.; Li, X.-L.; Watanabe, Y.; Wada, Y.; Takashima, T. 11C-cetrozole: an improved C-11C-methylated PET probe for aromatase imaging in the brain. *J. Nucl. Med.* **2014,** *55*, 852-857.

20. Hall, H.; Takahashi, K.; Erlandsson, M.; Estrada, S.; Razifar, P.; Bergström, E.; Långström, B. Pharmacological characterization of 18F‐labeled vorozole analogs. *J. Labelled Comp. Radiopharm.* **2012,** *55*, 484-490.
21. Tominaga, T.; Suzuki, T. Early phase II study of the new aromatase inhibitor YM511 in postmenopausal patients with breast cancer. Difficulty in clinical dose recommendation based on preclinical and phase I findings. *Anticancer Res.* **2002,** *23*, 3533-3542.
22. Baston, E.; Leroux, F. R. Inhibitors of steroidal cytochrome P450 enzymes as targets for drug development. *Recent Pat. Anti-Cancer Drug Discovery* **2007,** *2*, 31-58.
23. Watanabe, Y.; Onoe, H.; Takahashi, K.; Suzuki, M.; Doi, H.; Hosoya, T. Labeling compound for pet. In US Patents: 2010.
24. Okada, M.; Yoden, T.; Kawaminami, E.; Shimada, Y.; Kudoh, M.; Isomura, Y.; Shikama, H.; Fujikura, T. Studies on aromatase inhibitors. I. Synthesis and biological evaluation of 4-amino-4H-1, 2, 4-triazole derivatives. *Chem. Pharm. Bull.* **1996,** *44*, 1871-1879.
25. Adje, N.; Bonnet, P.; Carniato, D.; Delansorne, R.; Lafay, J.; Pascal, J.-C. New 1-N-phenylamino-1H-imidazole derivatives are aromatase inhibitors useful to treat e.g. estrogen-dependent tumors and benign or malignant tumors. Patent Number(s): US6737433-B1, **2004.**
26. Hansch, C.; Quinlan, J. E.; Lawrence, G. L. The LFER Between Partition Coefficients and the Aqueous Solubility of Organic Liquids. *J. Org. Chem.* **1968,** 33.
27. Hansch, C.; Björkroth, J. P.; Leo, A. Hydrophobicity and central nervous system agents: On the principle of minimal hydrophobicity in drug design. *J. Pharm. Sci.* **1987,** *76*, 663–687.
28. Ghosh, D.; Griswold, J.; Erman, M.; Pangborn, W. Structural basis for androgen specificity and oestrogen synthesis in human aromatase. *Nature* **2009,** *457*, 219-223.
29. Kao, Y. C.; Korzekwa, K. R.; Laughton, C. A.; Chen, S. Evaluation of the mechanism of aromatase cytochrome P450. *Eur. J. Biochem.* **2001,** *268*, 243-251.
30. Abadi, A. H.; Abou-Seri, S. M.; Hu, Q.; Negri, M.; Hartmann, R. W. Synthesis and biological evaluation of imidazolylmethylacridones as cytochrome P-450 enzymes inhibitors. *Med. Chem. Comm.* **2012,** *3*, 663-666.

31. Cavalli, A.; Recanatini, M. Looking for selectivity among cytochrome P450s inhibitors. *J. Med. Chem.* **2002,** *45*, 251-254.
32. Pingaew, R.; Prachayasittikul, V.; Mandi, P.; Nantasenamat, C.; Prachayasittikul, S.; Ruchirawat, S.; Prachayasittikul, V. Synthesis and molecular docking of 1, 2, 3-triazole-based sulfonamides as aromatase inhibitors. *Bioorg. Med. Chem.* **2015,** *23*, 3472-3480.
33. Zoraghi, R.; Francis, S. H.; Wood, D.; Bischoff, E.; Hütter, J.; Knorr, A.; Niedbala, M.; Enyedy, I.; Pomerantz, K.; Corbin, J. D. Tyrosine-612 in PDE5 contributes to higher affinity for vardenafil over sildenafil. *Int. J. Impot. Res.* **2006,** *18*, 413-413.
34. Egbuta, C.; Lo, J.; Ghosh, D. Mechanism of inhibition of estrogen biosynthesis by azole fungicides. *Endocrinology* **2014,** *155*, 4622-4628.
35. Sakata, I.; Tanaka, T.; Yamazaki, M.; Tanizaki, T.; Zheng, Z.; Sakai, T. Gastric estrogen directly induces ghrelin expression and production in the rat stomach. *J. Endocrinol.* **2006,** *190*, 749-757.
36. Kellokoski, E.; Pöykkö, S. M.; Karjalainen, A. H.; Ukkola, O.; Heikkinen, J.; Kesäniemi, Y. A.; Hörkkö, S. Estrogen replacement therapy increases plasma ghrelin levels. *J. Clin. Endocrinol. Metab.* **2005,** *90*, 2954-2963.
37. Makovey, J.; Naganathan, V.; Seibel, M.; Sambrook, P. Gender differences in plasma ghrelin and its relations to body composition and bone – an opposite - sex twin study. *Clin. Endocrinol.* **2007,** *66*, 530-537.
38. Kirilovas, D.; Naessen, T.; Bergström, M.; Bergström-Petterman, E.; Carlström, K.; Långström, B. Characterization of [11C] vorozole binding in ovarian tissue in rats throughout estrous cycle in association with conversion of androgens to estrogens in vivo and in vitro. *Steroids* **2003,** *68*, 1139-1146.
39. Stocco, C. Aromatase expression in the ovary: hormonal and molecular regulation. *Steroids* **2008,** *73*, 473-487.
40. Kobayashi, H.; Yoshida, S.; Sun, Y. J.; Shirasawa, N.; Naito, A. Changes of gastric aromatase and portal venous 17β-estradiol during the postnatal development and estrus cycle in female rats. *Endocrine* **2014,** *46*, 605-614.

41. Roselli, C. E.; Abdelgadir, S. E.; Rønnekleiv, O.; Klosterman, S. A. Anatomic distribution and regulation of aromatase gene expression in the rat brain. *Biol. Reprod.* **1998,** *58*, 79-87.
42. Tabatadze, N.; Sato, S. M.; Woolley, C. S. Quantitative analysis of long-form aromatase mRNA in the male and female rat brain. *PloS one* **2014,** *9*, e100628.
43. Jakab, R.; Horvath, T.; Leranth, C.; Harada, N.; Naftolin, F. Aromatase immunoreactivity in the rat brain: gonadectomy-sensitive hypothalamic neurons and an unresponsive "limbic ring" of the lateral septum-bed nucleus-amygdala complex. *J. Steroid Biochem. Mol. Biol.* **1993,** *44*, 481-498.
44. Zhang, Q.-G.; Wang, R.; Tang, H.; Dong, Y.; Chan, A.; Sareddy, G. R.; Vadlamudi, R. K.; Brann, D. W. Brain-derived estrogen exerts anti-inflammatory and neuroprotective actions in the rat hippocampus. *Mol. Cell. Endocrinol.* **2014,** *389*, 84-91.
45. Dief, A. E.-E.; Caldwell, J.; Jirikowski, G. Colocalization of P450 aromatase and oxytocin immunostaining in the rat hypothalamus. *Horm. Metab. Res.* **2013,** *45*, 273-276.
46. Fedele, L.; Somigliana, E.; Frontino, G.; Benaglia, L.; Vigano, P. New drugs in development for the treatment of endometriosis. *Expert Opin. Invest. Drugs* **2008,** *17*, 1187-202.
47. Wozniak, A.; Hutchison, R. E.; Morris, C. M.; Hutchison, J. B. Neuroblastoma and Alzheimer's disease brain cells contain aromatase activity. *Steroids* **1998,** *63*, 263-267.
48. Márquez‐Garbán, D. C.; Chen, H. W.; Goodglick, L.; Fishbein, M. C.; Pietras, R. J. Targeting Aromatase and Estrogen Signaling in Human Non‐Small Cell Lung Cancer. *Ann. N. Y. Acad. Sci.* **2009,** *1155*, 194-205.
49. Sarachana, T.; Xu, M.; Wu, R.-C.; Hu, V. W. Sex hormones in autism: androgens and estrogens differentially and reciprocally regulate RORA, a novel candidate gene for autism. *PloS one* **2011,** *6*, e17116.
50. Okada, M.; Yoden, T.; Kawaminami, E.; Shimada, Y.; Masafumi, K.; Isomura, Y. Studies on Aromatase Inhibitors. III. Synthesis and Biological Evaluation of

((4-Bromobenzyl)(4-cyanophenyl) amino) azoles and Their Azine Analogs. *Chem. Pharm. Bull.* **1997,** *45*, 482-486.

51. Lo, J.; Di Nardo, G.; Griswold, J.; Egbuta, C.; Jiang, W.; Gilardi, G.; Ghosh, D. Structural basis for the functional roles of critical residues in human cytochrome P450 aromatase. *Biochemistry* **2013,** *52*, 5821-5829.
52. Trott, O.; Olson, A. J. AutoDock Vina: improving the speed and accuracy of docking with a new scoring function, efficient optimization, and multithreading. *J. Comput. Chem.* **2010,** *31*, 455-461.

Table of Contents graphic

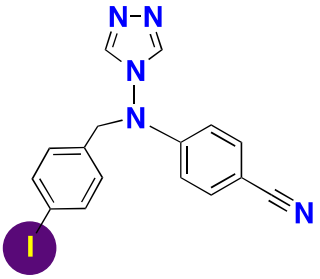

Aromatase Inhibitor, **5**
Binding Affinity IC_{50} = 0.17 nM

Ex vivo autoradiography mapping of aromatase enzyme in rats after iv injection of [^{125}I]**5**